# A Reconfigurable Solar Photovoltaic Grid-Tied Inverter Architecture for Enhanced Energy Access in Backup Power Applications

D. Venkatramanan, *Student Member, IEEE*, and Vinod John, *Senior Member, IEEE*

***Abstract*—In this article, a photovoltaic (PV) reconfigurable grid-tied inverter (RGTI) scheme is proposed. Unlike a conventional grid-tied inverter (GTI) that ceases operation during a power outage, the RGTI is designed to act as a regular GTI in the on-grid mode but it is reconfigured to function as a dc–dc charge-controller that continues operation during a grid outage. During this period, the RGTI is tied to the battery-bank of an external uninterruptible power supply (UPS)-based backup power system to augment it with solar power. Such an operation in off-grid mode without employing high-bandwidth communication with the UPS is challenging, as the RGTI control must not conflict with the battery management system of the UPS. The hardware and control design aspects of this requirement are discussed in this article. A battery emulation control scheme is proposed for the RGTI that facilitates seamless functioning of the RGTI in parallel with the physical UPS battery to reduce its discharge current. A system-level control scheme for overall operation and power management is presented to handle the dynamic variations in solar irradiation and UPS loads during the day, such that the battery discharge burden is minimized. The design and operation of the proposed RGTI system are independent of the external UPS and can be integrated with an UPS supplied by any manufacturer. Experimental results on a 4 kVA hardware setup validate the proposed RGTI concept, its operation, and control.**

***Index Terms*—Battery, closed-loop control, dual-mode inverters, grid-tied inverters (GTIs), solar photovoltaic (PV), uninterruptible power supply (UPS).**

## I. Introduction

GRID integration of renewable energy (RE) based distributed energy resources (DERs) has gained significant importance lately owing to the ever-increasing energy demand [1], [2]. A power-electronic interface is invariably required for this purpose and such a pulsewidth modulated (PWM) converter is referred to as the grid-tied inverter (GTI) [3], [4]. Solar photovoltaics (PV)-based GTI systems have garnered significant attention owing to their relative advantages such as direct static energy conversion and ease of integration [5], [6]. In the event of a grid outage, a conventional GTI is designed to detect an island formation and disconnect from grid to cease DER operation [7], [8]. This functionality is in compliance with the anti-islanding requirements laid out by IEEE 1547-2018 standard [9]. Thus, the conventional GTI by design is incapable of harnessing the available solar energy during a grid outage period, and hence, the RE resource along with the converter resources remains unutilized.

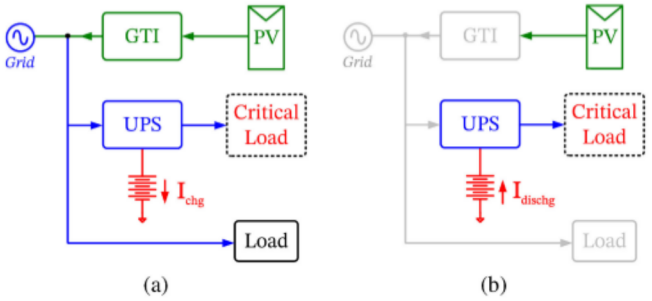


Fig. 1. Functional block schematic of a conventional GTI and UPS showing (a) on-grid mode and (b) off-grid mode.

Static uninterruptible power supply (UPS) system is conventionally employed to tackle power interruptions, which function only during grid outages to provide the necessary backup power to critical loads by discharging its battery bank [10], [11]. It can, thus, be noted that while the GTI ceases to operate during a grid outage, the UPS operation for backup power is initiated only after the detection of outage. This functional difference between the GTI and UPS is schematically shown in Fig. 1, where the UPS is unable to utilize the PV energy during outage while discharging the battery to support critical loads.

In order to utilize the PV resource during a grid outage, hybrid PV architectures, which combine the functionalities of GTI and UPS, have been explored in the literature [12]–[15]. Such hybrid PV systems combine the PV with a suitable battery storage system to tackle power outages, are also known as multiport dual-mode inverters [16], [17]. These systems are capable of operating in both on-grid and off-grid modes, and the schematic of such a system is shown in Fig. 2(a). In [12] and [13], a power

Manuscript received May 14, 2019; revised October 12, 2019; accepted December 4, 2019. Date of publication December 24, 2019; date of current version August 18, 2020. This work was supported by Central Power Research Institute (CPRI), Ministry of Power, Government of India, under the project "Power conversion, control, and protection technologies for microgrid." *(Corresponding author: D. Venkatramanan.)*

D. Venkatramanan and Vinod John are with the Department of Electrical Engineering, Indian Institute of Science, Bangalore 560012, India (e-mail: venkat86ram@gmail.com; vjohn@iisc.ac.in).

Color versions of one or more of the figures in this article are available online at http://ieeexplore.ieee.org.

Digital Object Identifier 10.1109/TIE.2019.2960742

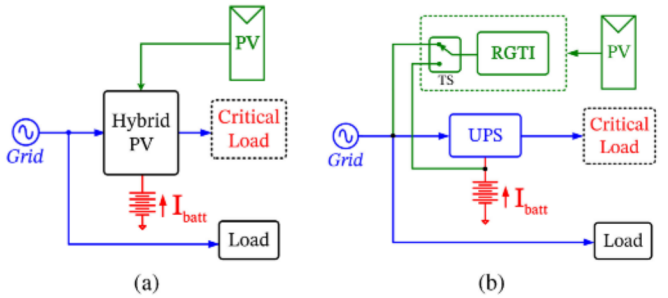


Fig. 2. Block schematic of (a) hybrid PV system and (b) proposed RGTI system.

circuit architecture with individual converters for PV, battery, and grid is proposed, while in [14], a control scheme based on instantaneous power balance theory is proposed for such a system that does not require exclusive determination of modes for operation and control. Additionally, battery management is performed along with an adaptive tolerance band based maximum power point tracking (MPPT) algorithm. In [15], a load priority based control strategy is proposed for operation and power management in a hybrid PV-based UPS. In [17], a control strategy for a single-stage dual-mode inverter that acts as an ac microgrid is presented. In [18], the hybrid PV system is extended to include a wind energy input and an active–reactive power control method is proposed for stable system operation when it is disconnected from the grid. A similar system is considered in [19], where an improved perturb and observe (P&O) algorithm is suggested for such a multi-input system. In many of these works, the coupling of various power conversion stages that interact with battery, PV, and grid takes place inside the system at the common dc bus. Alternatively, there are hybrid PV systems that adopt ac-coupling technique, where the PV inverter gets tied to the ac bus at the output side [20], [21].

The hybrid PV architectures discussed in the literature adopt an integrated design approach and achieve the desired objective of harnessing solar energy during a power outage with superior control performance. However, they also carry certain limitations.

1) Retrofitting and upgrading an existing UPS backup system with PV capability is not feasible. Many facilities typically tend to have a backup power source that is previously installed. The hybrid-PV approach requires a complete replacement of the existing backup system, and thus requiring a system-level change in the electrical system of the facility.
2) Also, depending on the battery voltage ratings of the existing UPS, a replacement of battery-bank may also be necessitated when a hybrid-PV system is newly installed, as it is not recommended to combine aged batteries with new ones. It is typically recommended to use batteries of same AH capacity, type, age, and manufacturer owing to reliability and cycle-life considerations [22]. Replacement of battery-banks is typically expensive.
3) Scaling up of PV capacity without impacting or requiring a change in the balance of system is not feasible in the hybrid-PV approach due to its integrated design.

In view of the above, a novel reconfigurable GTI (RGTI) architecture is proposed in this work, whose block schematic is shown in Fig. 2(b). In this approach, the UPS and the GTI are functionally combined while keeping the actual systems physically separate and independent in terms of design and control. The proposed RGTI acts as a regular dc–ac GTI when grid is present, but reconfigures as a dc–dc charge-controller during a grid outage and interacts with the battery-bank of the external UPS. Such a dc-coupled operation of the RGTI augments the UPS with solar power and, hence, brings PV capability to an existing backup power system. However, operation of RGTI in grid-disconnected mode in tandem with a generic external UPS, without having high-bandwidth communication or data-exchange with the UPS controller, poses technical challenges. The RGTI should not overcharge the battery or interfere with the algorithms of battery management system (BMS) present in the UPS. Hence, suitable circuit-level as well as a system-level controls are essential for operating the RGTI with the UPS, which is the focus of this article.

The contributions of this article are as follows. An RGTI scheme is proposed that enhances the capability of a conventional GTI leading to enhanced utilization of solar energy during grid outage. In order to achieve this objective, a dc-coupled operating scheme for such a system is proposed in this work, where an additional battery-tied mode of operation is employed aside from the conventional grid-tied mode. In this mode, the RGTI is operated as a dc–dc charge-controller and, unlike a conventional design that always operates in MPPT mode, a new battery emulation mode is also proposed for the RGTI, to support the external UPS battery with solar energy. A battery-current control scheme is proposed for emulating a high ampacity battery using a PV source such that the critical load is supplied by the PV source when the irradiation is adequate. Such an operation of the RGTI in tandem with the UPS ensures that the discharge burden on the physical battery is minimized, thus leading to enhanced cycle life and the overall backup system life. The circuit-level controls for battery emulation and MPPT are presented. In order to tackle the dynamic variations in the UPS load and ambient solar irradiation and to decide on the system operating mode, a system-level control scheme is presented that functions without requiring high-bandwidth communication between the RGTI and UPS. This ensures that the UPS operation and its BMS for battery maintenance are not affected by the RGTI operation. Experimental results on a 4 kVA hardware setup validate the operation and control of the RGTI in on-grid as well as off-grid mode. The proposed system architecture allows independent design and control of the RGTI, thus providing retrofitting ability to upgrade an existing UPS with PV capability, independent of its ratings and manufacturer. Such a reconfigurable solution, thus, addresses the drawbacks of the conventional GTI systems and facilitates enhanced solar energy access and resource utilization, similar to a hybrid-PV solution, while also providing features of retrofitting PV and its flexible scaling, to extend the cycle life of the local UPS batteries.

The remainder of the article is organized as follows. The coupling mechanisms of the GTI with the UPS are evaluated in Section II. The proposed RGTI architecture is presented in

Section III, along with its circuit modeling and transfer-function analysis in Section IV. The grid-tied mode of operation is briefly described in Section V. The battery-tied mode of operation along with the proposed battery emulation control (BEC) scheme is discussed in Section VI. A brief description of the MPPT control employed is provided in Section VI-C, followed by the description of the circuit-level and system-level control designs in Section VI-C and VIII, respectively. Experimental results on a hardware setup consisting of a 4 kVA RGTI and a 5 kVA commercial UPS are presented in Section IX, and Section X concludes this article.

## II. Evaluation of Coupling Mechanisms

Standard operation of a PV GTI system is as shown in Fig. 1. It is intended that the GTI is not kept idle and continues to operate and harvest solar energy during a grid outage. Hence, the GTI is coupled and operated in tandem with an external UPS. In this section, the mechanisms for coupling the GTI with the external UPS in off-grid mode are compared and the proposed scheme for the RGTI is explained.

### A. AC-Coupling

In *ac-coupling* scheme, the GTI is connected on the ac side of the UPS to share the load. In case the PV inverter is operated in voltage control mode, the UPS should be compatible for power converter paralleling in a decentralized manner. However, all UPS types may not support such a paralleling feature. On the other hand, instead of voltage control mode, if the GTI treats the UPS output as a virtual grid and interacts with the same in current control mode, then the excess power generated by the inverter during MPPT must be absorbed by the UPS to charge the battery under light UPS loading conditions. This would not only require bidirectional power flow capability in the UPS power circuit along with supporting firmware controls, but also communication of the necessary information and data between the two digital controllers. This is essential to allow such an operation without tripping the UPS. Thus, ac-coupling imposes specific hardware and firmware constraints on the UPS for compatible operation. Since varied power circuit topologies exist in UPS designs [10], [11], [23], it is not possible to assume that the UPS by default would permit such bidirectional power flows and paralleling features. Thus, operation of a GTI with a generic UPS through ac-coupling can lead to system tripping or potential damage. Hence, this is not suitable for an independent and reconfigurable operation of the GTI without requiring high-bandwidth communication links.

### B. Dc-Coupling

If *dc-coupling* on the battery side is employed, then the GTI and the UPS systems are decoupled in terms of operation and control, as the battery behaves as a stiff voltage source. Hence, integration of the GTI and the battery can be readily done, especially at medium power levels where the UPS battery voltage is of the order of 100 V and above. This configuration alleviates the compatibility issues between the two systems, and hence independent design and operation of the GTI and UPS are feasible without requiring high-bandwidth communication, unlike ac coupled systems. However, a suitable control mechanism is necessary for the off-grid GTI operation, which is discussed in Section III.

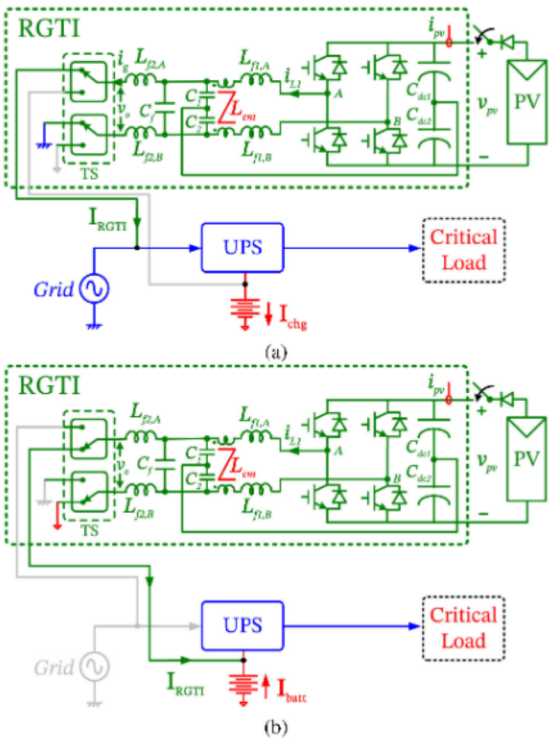


Fig. 3. Circuit schematic of the proposed RGTI functional scheme showing (a) on-grid mode and (b) off-grid mode.

## III. Proposed RGTI System

### A. System Configuration

The circuit schematic of the RGTI system configuration for single-phase single-stage PV application is shown in Fig. 3. It comprises an H-bridge inverter with unipolar PWM, differential-mode *LCL*-filter, common-mode (CM) *LC*-filter and a transfer-switch TS that enables changeover from grid to battery and vice versa. The CM filter is essential to meet the leakage current requirements of a PV inverter [24]. Such a hardware configuration is compatible for both dc–ac inversion and dc–dc conversion, which is leveraged in the RGTI for off-grid mode operation.

### B. System Operation

The RGTI system has two operating modes, depending on the availability of grid.

***1) Grid-Tied Mode:*** When the grid is present, the RGTI is tied to the grid and controlled to feed maximum PV power, just as a regular GTI [4], [7]. The circuit schematic in this mode is shown in Fig. 3(a). The converter is controlled such that MPPT is performed while maintaining sinusoidal injected grid current with the desired unity power factor [25].

***2) Battery-Tied Mode:*** In the event of a grid outage, the RGTI transitions into the battery-tied mode where it is tied to the external UPS battery and operates as a dc–dc converter. The

corresponding circuit schematic is shown in Fig. 3(b). Similar to the grid-tied case, if MPPT is performed continuously by the RGTI to provide energy support, then depending on the UPS loading condition, PV generation capacity and the irradiation level, the battery may discharge to deliver power or charge and absorb power. This depends on the level of mismatch between generated PV power and the UPS load consumption. Continuous MPPT operation of the RGTI may overcharge the UPS battery during light load conditions and excess PV generation, thus leading to battery damage. However, employing a battery management control in the RGTI also interferes with the BMS algorithm present within the UPS, and such a clash can also lead to poor battery management that affects the life of the storage elements. This is undesirable and, hence, a second mode of RGTI operation is necessary that complements the MPPT and allows solar energy access during outage. This second mode is required to ensure that only adequate support is rendered by the RGTI depending on the UPS loading condition when the PV generation is high. To achieve this objective, a battery emulation mode is proposed that ensures that the discharge burden on the battery is minimized through solar power.

Thus, the RGTI is controlled in two submodes in battery-tied mode, namely, 1) MPPT and 2) BEC, and the transitions between these two submodes are governed by the level of UPS loading and the ambient irradiation conditions. These mode-transitions are discussed in detail in Section VIII. In MPPT mode, a voltage-based P&O algorithm is employed to extract maximum PV power. In BEC mode, the RGTI is controlled in such a manner that the battery current is regulated to zero irrespective of variations in the UPS load as long as adequate solar irradiation is available to achieve the same. This is a critical requirement as the RGTI should not overcharge the battery during these dynamic conditions. This is discussed further in Section VI.

A system-level supervisory control scheme is required to govern the transitions between grid-tied and battery-tied modes as well as that between the submodes. The conditions for transition are dependent on the availability of the grid, the UPS loading, and the ambient irradiation conditions. This is discussed in detail in Section VIII.

## IV. Circuit Modeling and Analysis

For the design of circuit-level controllers of the RGTI in the individual submodes, a suitable circuit model is essential for carrying out transfer-function analysis. The models for control design in grid-connected mode are well discussed in literature [4], [7], [25]. In this section, the RGTI functioning in the proposed battery-tied mode is analyzed and a small-signal linear model for control design is obtained. The RGTI circuit schematic is shown in Fig. 4(a). The governing equations of the system are as follows. During the on-period $T_{\text{on}} = dT_s$

$$v_{\text{pv}} = L_{f1}\frac{di_{L1}}{dt} + i_{L1}r_1 + v_c, \quad C_f\frac{dv_c}{dt} = i_{L1} - i_{L2} \tag{1}$$

$$i_{\text{pv}} - i_{L1} = C_{\text{dc}}\frac{dv_{\text{pv}}}{dt}, \quad v_c - v_B = L_{f2}\frac{di_{L2}}{dt} + i_{L2}r_2. \tag{2}$$

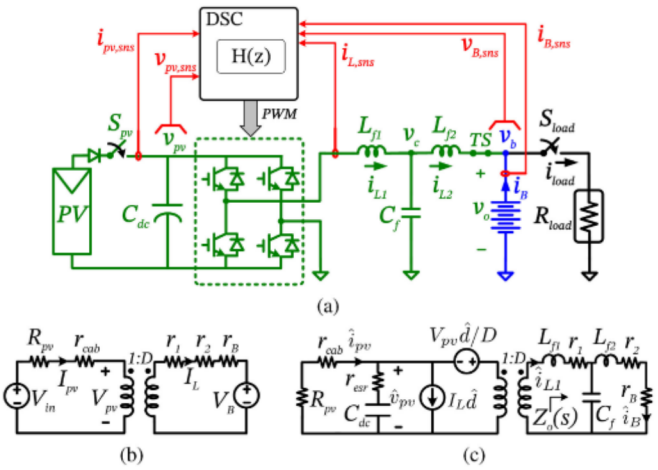


Fig. 4. Circuit model of the RGTI in battery-tied mode showing (a) equivalent circuit schematic, (b) static dc model, and (c) small-signal dynamic ac model with parasitic resistances.

During the off-period $T_{\text{off}} = (1-d)T_s$

$$0 = L_{f1}\frac{di_{L1}}{dt} + i_{L1}r_L + v_c, \quad C_f\frac{dv_c}{dt} = i_{L1} - i_{L2} \tag{3}$$

$$i_{\text{pv}} = C_{\text{dc}}\frac{dv_{\text{pv}}}{dt}, \quad v_c - v_B = L_{f2}\frac{di_{L2}}{dt} + i_{L2}r_2. \tag{4}$$

The circuit averaging technique discussed in [26] is applied to the above equations using small-signal perturbations in the circuit variables, which yields the static dc model and the corresponding small-signal ac model of the RGTI circuit that are shown in Fig. 4(b) and (c), respectively, that includes the circuit parasitic resistances in the filter components, battery, PV source, and the interconnecting cable. From the dc model, the steady-state operating points of circuit quantities for a quiescent duty-ratio $D$ are given by

$$I_{\text{pv}} = DI_{L1}, \quad I_{L1} = \frac{DV_{\text{in}} - V_B}{D^2R_{\text{in}} + R_o}, \quad V_{\text{pv}} = V_{\text{in}} - I_{\text{pv}}R_{\text{in}} \tag{5}$$

where, $R_{\text{in}} = R_{\text{pv}} + r_{\text{cab}}$ and $R_o = r_1 + r_2 + r_B$. For the transfer-function analysis, the perturbation in duty $\hat{d}$ is the only small-signal input considered in the system as shown in Fig. 4(c), where the perturbations $\hat{v}_{\text{in}}$ and $\hat{v}_B$ in the input source and battery voltages are assumed to be zero. Since the battery behaves as a stiff voltage source with negligible internal resistance $r_B$, the parallel combination of battery and the load resistance $R_{\text{load}}$ is equivalently modeled as a resistor $r_B$ in the dc and ac equivalent circuit. Furthermore, the filter capacitor $C_f$ of the output $LCL$ filter can be designed such that the resonance caused lies beyond the frequency range of control interest. This leads to a model-order reduction, where the effect of $C_f$ can be made negligible for control analysis and bandwidth selection. The secondary side output filter impedance $Z_o(s)$, thus, is simplified as

$$Z_o(s) = sL_{f1} + r_1 + \frac{sL_{f2} + r_2 + r_B}{(sL_{f2} + r_2 + r_B)sC_f + 1} \tag{6}$$

$$\Rightarrow Z_o(s) \approx sL_{f1} + r_1 + sL_{f2} + r_2 + r_B = sL_f + R_o \tag{7}$$

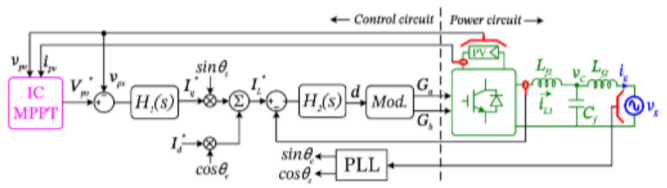


Fig. 5. Control schematic of RGTI operating in grid-tied mode performing MPPT.

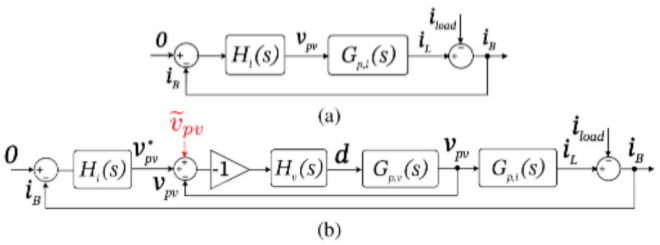


Fig. 6. BEC schemes showing (a) basic current-control and (b) modified two-loop control.

where $L_f = L_{f1} + L_{f2}$. Using (7) in the ac circuit model, the resulting dc-bus voltage $\hat{v}_{\rm pv}$ to control duty $\hat{d}$ transfer-function is obtained as

$$G_{p,v}(s) = \frac{\hat{v}_{\rm pv}(s)}{\hat{d}(s)} = k_a \frac{(1+s/\omega_c)(1+s/\omega_d)}{(1+s/\omega_a)(1+s/\omega_b)}. \quad (8)$$

The resulting perturbations in the battery and inductor currents $\hat{i}_B$, $\hat{i}_{L1}$, and $\hat{i}_{L2}$ are equal within the control bandwidth. The corresponding transfer-functions with respect to dc-bus voltage $\hat{v}_{\rm pv}$ are derived as

$$G_{p,i}(s) = \frac{\hat{i}_B(s)}{\hat{v}_{\rm pv}(s)} = \frac{\hat{i}_{L1}(s)}{\hat{v}_{\rm pv}(s)} = k_b \frac{1+s/\omega_b}{(1+s/\omega_c)(1+s/\omega_d)} \quad (9)$$

$$k_a = -R_{\rm in}\left(\frac{2DV_{\rm pv} - V_B}{D^2R_{\rm in} + R_o}\right),\ k_b = \frac{-1}{R_{\rm in}}\left(\frac{V_{\rm pv} - I_{\rm pv}R_{\rm in}}{2DV_{\rm pv} - V_B}\right) \quad (10)$$

$$\omega_a = \frac{D^2R_{\rm in} + R_o}{L_f}, \quad \omega_b = \frac{1}{R_{\rm in}C_{\rm dc}} \quad (11)$$

$$\omega_c = \omega_a\left(\frac{2DV_{\rm pv} - V_B}{DV_{\rm in} - V_B}\right), \quad \omega_d = \frac{1}{r_{\rm esr}C_{\rm dc}}. \quad (12)$$

The inverter side inductor current $i_{L1}$ and the dc-bus voltage $v_{\rm pv}$ are the desired control variables for the RGTI as explained subsequently in Sections V and VI-A. Equations (8) and (9) form the plant transfer-functions that are used for the respective circuit-level control designs in battery-tied mode.

## V. Grid-Tied Mode

The control circuit schematic of the grid-tied mode is indicated in Fig. 5. The H-bridge inverter is synchronized with the grid using a resonant-integrator based phase locked loop (PLL) [4]. The grid voltage is aligned with the $q$-axis, which corresponds to the real power axis. The inverter current is treated as the inner control variable that is controlled using a proportional-resonant (PR) current-controller $H_2(s)$ that tracks the ac current reference command. The structure of the current-controller and voltage-controller is designed based on [27] and [28]. An intermediate voltage loop based on a proportional-integral (PI) controller $H_1(s)$ is present that regulates the PV bus voltage on the dc side. The voltage reference command to this loop is provided by an outer voltage-based incremental conductance (IC) MPPT controller. Such a three-loop control strategy for GTI is discussed in [25] and [29]. The respective control structures are given by

$$H_1 = k_{p1} + \frac{k_{i1}}{s}, \quad H_2 = k_{p2} + \frac{k_{r2}s/\omega_0}{1 + k_{r2}k_d s/\omega_0 + s^2/\omega_0^2}. \quad (13)$$

The bandwidths of current and voltage loops in grid-tied mode are designed to be 800 and 5 Hz, respectively, and the control parameters are listed in Table II.

## VI. Battery-Tied Mode

The circuit schematic for the study of battery-tied mode is shown in Fig. 4(a). For the purpose of analysis, the UPS and its output load are equivalently represented as a resistor $R_{\rm load}$ on the battery. The split differential mode filters in Fig. 3 are equivalently represented as a single-stage *LCL* filter.

### A. Battery Emulation Control

When two batteries are connected in parallel to feed a given load, the battery with higher ampacity takes the larger share of current. In order to emulate a battery using the RGTI, the control must ensure that the RGTI takes most of the load, such that the physical UPS battery current is minimized. Such a battery emulation scheme is feasible when the irradiation is adequate to cater to the complete UPS load, which minimizes battery discharge. This is achieved by operating the RGTI as a buck converter that regulates the battery current to zero.

This is performed by treating the battery current $i_B$ as the feedback variable and regulating it to zero using the single-loop current-control scheme as indicated in Fig. 6(a). In such a scheme, the reflected UPS load current $i_{\rm load}$ is treated as a disturbance variable that is rejected by $H_i(s)$, which is a PI current-controller that achieves zero steady-state error. The system transfer-functions can, thus, be derived as

$$\frac{i_B(s)}{i_{\rm load}(s)} = \frac{1}{1 + G_{p,i}H_i} = \frac{s}{(1+G_{p,i}k_{p,i})s + k_i} \quad (14)$$

where $G_{p,i}$ is derived in (9). In steady state, this yields $I_B = 0$. However, such a buck-mode operation is feasible only when the insolation is adequate to regulate $i_B$ to zero.

If the PV power capacity is inadequate to meet the load demand in BEC submode, the control loop will cause continuous decline of dc-bus voltage below undervoltage threshold, as the single-loop current-control structure operates independently with no information regarding the available PV power and the

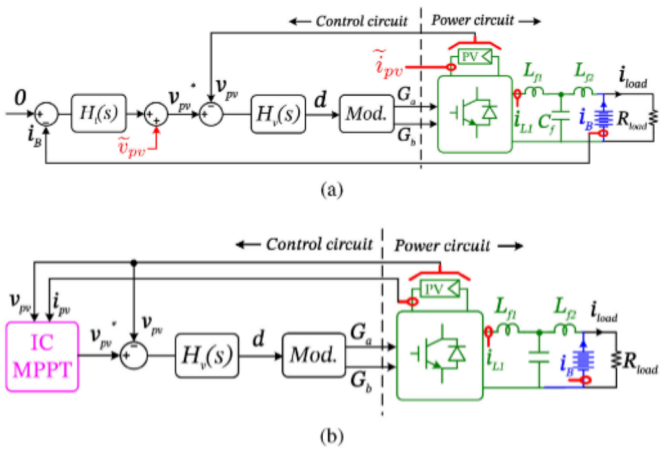


Fig. 7. Control schematic of RGTI in battery-tied mode showing (a) BEC and (b) voltage-based MPPT control.

margin that exists between this value and the load demand. This will trip the buck-converter system and the power converter will cease operation. Hence, a suitable mechanism is required to detect the power margin available between the PV capacity and the load demand for BEC to be feasible. Instead of employing external controllable loads or irradiation sensors, the necessary detection is performed through measured electrical variables with the aid of a modified control scheme, which is explained next.

### B. Modified Control for Power Margin Detection

It is essential to detect the change in power margin between the available peak PV power and the UPS load power, and take necessary action in order to operate the RGTI system continuously. Also, it is desirable to perform this without the use of expensive irradiation sensors. In view of this, a modified two-loop control structure is proposed, as indicated in Fig. 6(b), that facilitates estimation of power margin with the aid of measured electrical circuit variables. The modified control scheme consists of an inner PV bus voltage loop and the outer battery current loop.

A perturbation $\widetilde{v}_{\rm pv}$ is introduced in the inner voltage loop and the corresponding perturbation in PV current $\widetilde{i}_{\rm pv}$ is measured. This is indicated in the circuit schematic of modified control shown in Fig. 7(a). The ratio of the two quantities yields the IC $\widetilde{g}$ of the operating point of the PV [30], while catering to a given UPS load in BEC mode. The ratio of dc PV current $I_{\rm pv}$ to voltage $V_{\rm pv}$ in this condition yields the static conductance $G_{\rm dc}$ of the PV. The ratio of these conductances $G_r$ is given by

$$\widetilde{g} = \left|\frac{\widetilde{i}_{\rm pv}}{\widetilde{v}_{\rm pv}}\right|, \quad G_{\rm dc} = \frac{I_{\rm pv}}{V_{\rm pv}}, \quad G_r = \frac{\widetilde{g}}{G_{\rm dc}} = \left|\frac{\widetilde{i}_{\rm pv}}{\widetilde{v}_{\rm pv}}\right| \frac{V_{\rm pv}}{I_{\rm pv}}. \tag{15}$$

The conductance ratio $G_r$ provides an estimate of the difference between the available maximum power point (MPP) of the PV and the operating power point (OPP) for a given UPS load and irradiation condition, as explained below. A high $G_r$ value indicates that the PV is operating near open circuit condition (OCC), thus indicating a large margin between MPP and OPP. When OPP = MPP, $G_r$ is unity and indicates MPPT operation. When $G_r$ is close to zero, it indicates that OPP is present in the current limited region of PV close to short-circuit condition [30].

Hence, by continuously monitoring $G_r$, the drift in the PV operating point toward MPP and a subsequent reduction in power margin between PV capacity and load demand can be detected. The system-level control uses this information to handle the dynamic changes in solar irradiation and UPS loading, and when the available margin is inadequate to continue BEC operation, the RGTI system is steered out of BEC and is transitioned into MPPT submode. In this condition, the battery effectively discharges when the UPS is catering the load. However, the discharge burden is reduced as the RGTI is providing maximum support from the PV. When the irradiation increases and enhances the PV capacity sufficiently, the system-level control detects the same and steers the system back into BEC submode. The mode-transitions between BEC and MPPT submodes are detailed in Section VIII.

### C. Maximum Power Point Tracking

The control structure for MPPT operation in battery-tied mode is shown in Fig. 7(b). A voltage-based MPPT controller that uses IC algorithm is employed that provides stable tracking performance, which is well established in the literature [30]–[32]. It can be seen that this structure is similar to that indicated in Fig. 7(a), but voltage reference $v^*_{\rm pv}$ in this case is commanded by the MPPT algorithm unlike the BEC mode. The PV bus voltage-controller design is, thus, common to both BEC and MPPT modes.

## VII. Circuit-Level Control Design

The circuit-level controls for grid-tied inverter operation is well established in literature as discussed in Section V. Hence, this section aims at the design of controls essential for the proposed battery-tied operating mode of the RGTI. For the design of inner PV voltage control loop whose small-signal equivalent circuit is shown in Fig. 6(b), a PI-controller $H_v$(s) is chosen that provides the required control-duty $d(s)$ to yield zero steady-state error. Hence, the plant $G_{p,v}$ for the inner loop is given by (8) as indicated below

$$G_{p,v} = \frac{\hat{v}_{\rm pv}(s)}{\hat{d}(s)}, \quad H_v = -\left(k_{p,v} + \frac{k_{i,v}}{s}\right). \tag{16}$$

It can be noted that $H_v(s)$ carries an inversion, which is to offset the negative dc gain of the plant $G_{p,v}$ and ensure closed-loop control stability. The zero of the PI-controller is selected such that it cancels the plant pole $\omega_b$. For the system parameters indicated in Table I, the plant zeros $\omega_c$ and $\omega_d$ lie outside the frequency range of control interest, and, hence, can be removed for analytical design. The resultant loop-gain $T_v(s)$ and closed-loop transfer-function $G_{c,v}$(s) are given by

$$T_v(s) = \frac{k_a k_{i,v}}{s(1+s/\omega_a)}, \quad G_{c,v}(s) = \frac{\omega_a k_a k_{i,v}}{s^2 + \omega_a s + \omega_a k_a k_{i,v}}. \tag{17}$$

This loop serves the purpose of both MPPT and BEC modes of RGTI operation as explained in Section VI-C, and is designed to have a bandwidth of $f_{{\rm bw},v} = 55$ Hz and phase margin of 35°.

TABLE I
SYSTEM RATINGS AND PARAMETERS

| Item | Value |
|---|---|
| Converter rating | 4 kVA |
| Grid voltage | 220 V |
| PV power rating | 3.6 kW |
| PV voltage $V_{pv}$ | 480 V |
| Battery voltage $V_B$ | 192 V |
| Battery Ampacity $C$ | 60 Ah |
| $C_{dc}$, $r_{esr}$ | 1200 $\mu F$, 80 $m\Omega$ |
| $f_{sw}$ | 10 kHz |
| $L_{f1}$, $L_{f2}$ | 1 mH |
| $C_f$ | 4 $\mu F$ |

TABLE II
RGTI CONTROL PARAMETERS

| Item | Value | Item | Value |
|---|---|---|---|
| $k_{p,v}$ | $0.004167V^{-1}$ | $k_{i,v}$ | $2.08333\ V^{-1}s^{-1}$ |
| $k_{i,i}$ | $50\ A^{-1}s^{-1}$ | $k_{p2}$ | $15\ A^{-1}$ |
| $k_{r2}$ | 2000 | $k_d$ | 0.001 |
| $k_{p1}$ | $0.1\ AV^{-1}$ | $k_{i1}$ | $5\ AV^{-1}s^{-1}$ |

For the outer current regulation loop in BEC mode, the controller $H_i(s)$ provides the PV bus voltage reference $v^*_{\text{pv}}$ as indicated in Fig. 7(a) for regulating $i_B$ to zero. Hence, the plant for the outer loop is given by (9). The controller $H_i(s)$ comprises of an integrator for ensuring zero steady-state error, whose gain $k_{i,i}$ is chosen to achieve the desired bandwidth. Within the frequency range of control interest, these expressions along with the loop-gain $T_i(s)$ are

$$G_{p,i} = \frac{\hat{i}_B(s)}{\hat{v}_{\text{pv}}(s)},\quad H_i = \frac{k_{i,i}}{s},\quad T_i(s) = k_{i,i}k_b\omega_b\frac{1+s/\omega_b}{s}. \tag{18}$$

The corresponding closed-loop transfer-function $G_{c,i}$(s) is obtained as

$$G_{c,i}(s) = \frac{s+\omega_b}{s(k_bk_{i,i}+\omega_b)+\omega_bk_bk_{i,i}}. \tag{19}$$

The current loop bandwidth is selected such that small-signal perturbation $\tilde{v}_{\text{pv}}$ of 10 Hz introduced in the inner loop, for the measurement of $G_r$ as indicated in Section VI-B, is not rejected by the control action. Hence, the bandwidth is set to $f_{\text{bw},i} = 0.5$ Hz. The corresponding RGTI control parameters for the voltage and current loops are listed in Table II.

## VIII. SYSTEM-LEVEL CONTROL DESIGN

In order to facilitate enhanced energy access during outage using the RGTI, a system-level control system is essential in order to steer the RGTI between the various operating modes. The circuit-level controls for grid-tied and battery-tied modes are described in Sections V and VI, respectively. In this section, the system-level operation of the RGTI under dynamic variations of the UPS load, solar irradiation, and grid condition is described. The decision on operating mode or state of the RGTI along with the associated mode-transitions are made using three decision variables $G_r$, $i_B$, and $v_g$, that are continuously measured online by the digital signal controller (DSC). Correspondingly, the flags $f_{\text{grid}}$, $f_{\text{chg}}$, and $f_G$ are set to indicate the conditions of grid, battery charge/discharge, and conductance ratio $G_r$, respectively. The status of these variables are indicated in Table III, and the mode-transition logic is explained next.

TABLE III
THRESHOLD CONDITIONS AND STATUS OF MEASURED DECISION VARIABLES FOR BATTERY-TIED RGTI STATE-TRANSITIONS

| Flag | Status | Description |
|---|---|---|
| $f_G$ | L | $G_r < 4$, showing low PV power margin |
| $f_G$ | H | $4 < G_r < 1000$, showing high PV power margin |
| $f_{grid}$ | H | Grid voltage $v_g$ present |
| $f_{grid}$ | L | Grid voltage $v_g$ absent due to islanding |
| $f_{chg}$ | L | Battery discharges where $i_B > 0$ |
| $f_{chg}$ | H | Battery charges through MPPT where $i_B < 0$ |

TABLE IV
MODE-TRANSITION TABLE FOR RGTI SYSTEM OPERATION

| Condition | $f_{grid}$ | $f_{chg}$ | $f_G$ | Present Mode | Next Mode |
|---|---|---|---|---|---|
| 1 | H | - | - | $\mathbf{R_G}$ | $\mathbf{R_G}$ |
| 2 | L | - | - | $\mathbf{R_G}$ | $\mathbf{R_{B1}}$ |
| 3 | L | L | - | $\mathbf{R_{B1}}$ | $\mathbf{R_{B1}}$ |
| 4 | L | H | - | $\mathbf{R_{B1}}$ | $\mathbf{R_{B2}}$ |
| 5 | L | - | H | $\mathbf{R_{B2}}$ | $\mathbf{R_{B2}}$ |
| 6 | L | - | L | $\mathbf{R_{B2}}$ | $\mathbf{R_{B1}}$ |

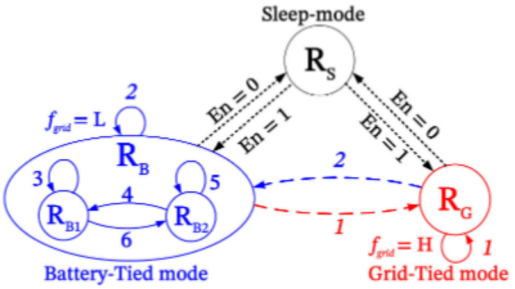


Fig. 8. Mode-transition diagram for RGTI operation.

### A. Mode-Transition Logic

The mode-transition table for the RGTI and the corresponding mode-transition diagram are shown in Table IV and Fig. 8, respectively. It can be noted that when the grid is present, $f_{\text{grid}} =$ H, the system functions in grid-tied mode and performs MPPT as represented by the mode $\mathbf{R_G}$ in *condition-1* in Table IV. This mode is marked in red in Fig. 8. When an islanding occurs, $f_{\text{grid}}$ turns low and the system transitions into battery-tied mode as indicated by *condition-2*, and this mode is marked in blue in Fig. 8. By default, the system enters the MPPT mode in this state, as indicated by $\mathbf{R_{B1}}$ in *condition-3*, and the status-monitoring of the battery charging flag $f_{\text{chg}}$ is initiated. If the MPPT power is lower than the operating UPS power, then the battery effectively discharges to deliver power. This is represented by $f_{\text{chg}} =$ L and the system continues to be in MPPT submode. However, when the load reduces under adequate irradiation condition such that MPPT operation tends to charge the battery by reversing the battery-current $i_B$, this suggests that the MPP or PV capacity is more than the load demand. In such a case, the flag $f_{\text{chg}}$ turns high ($f_{\text{chg}} =$ H) as indicated in Table III. This corresponds to *condition-4* in Table IV, and the system immediately transitions

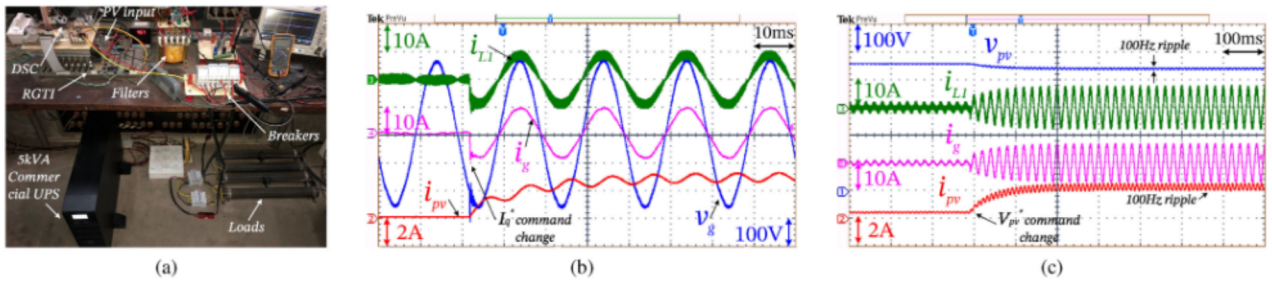


Fig. 9. (a) Hardware setup, and experimentally measured profiles of $v_{\text{pv}}$, $i_g$, $i_{L1}$, and $i_{\text{pv}}$ in grid-tied mode for (b) 40% step change in current loop reference $I_q^*$ for inner loop, (c) 10% step change in voltage loop reference $v_{\text{pv}}^*$.

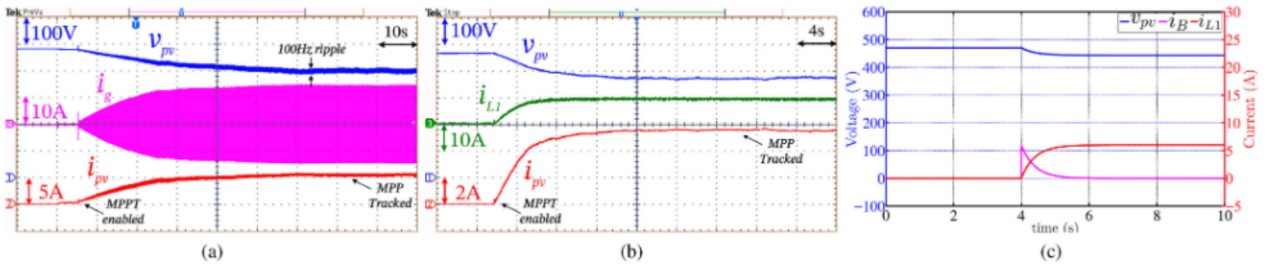


Fig. 10. (a) Experimental MPPT waveforms in grid-tied mode $R_G$, (b) Experimental MPPT waveforms in battery-tied submode $R_{B1}$, and (c) simulated battery-current dynamics in BEC submode $R_{B2}$ for a 30% step change in UPS load.

into BEC mode represented by $\mathbf{R_{B2}}$. Flag $f_G$ indicates the status of the conductance ratio while the system operates in BEC mode, as explained in Section VI-B. $f_G = \text{H}$ indicates a high PV power margin available between OPP and MPP, and the BEC mode of operation can continue. However, due to variations in the ambient irradiation or due to UPS load changes, if the power margin decreases below a preset threshold indicating a drift of OPP beyond MPP, $f_G$ turns low, and the system transitions back to MPPT mode $\mathbf{R_{B1}}$ as indicated by *condition-6*. Such an operation of the RGTI in battery-tied mode minimizes the discharge burden on the physical UPS battery. When the grid voltage is restored, the flag $f_{\text{grid}}$ turns high as indicated by *condition-1*, and the system transitions back to grid-tied mode. A sleep-state $R_s$ is present where the DSC is awake but the RGTI control is OFF. No power conversion takes place in this mode unless the flag $En$ is enabled, which moves the system out of sleep-state to initiate power transfer.

## IX. Experimental Validation

In this section, the proposed RGTI-based solution for backup power extension is experimentally validated. The hardware setup consisting of the RGTI converter, external 5 kVA commercial UPS, load resistances, and contactors is indicated in Fig. 9(a). The system parameters and ratings are listed in Table I. The system controls are implemented in a TMS320F28377S DSP-based DSC.

Fig. 9(b) shows the performance of the inner PR current-controller $H_2$ in grid-tied mode, for a 40% step change in real current reference $I_q^*$. As can be seen from the inverter current $i_{L1}$ and injected grid current $i_g$, the reference is swiftly tracked by the PR current-controller well within a quarter cycle. The high performance of the PR controller ensures a sinusoidal grid current that is devoid of switching frequency ripple due to the *LCL*-filter.

Fig. 9(c) shows the performance of the PV bus voltage-controller $H_1$ in grid-tied mode, for a command change in $v_{\text{pv}}^*$ of 10%. It can be seen that $v_{\text{pv}}$ settles in about 100 ms. A corresponding increase can be seen in the amplitudes of the PV current $i_{\text{pv}}$ and the grid current $i_g$.

Fig. 10(a) shows the MPPT performance of the RGTI in grid-tied mode $R_G$, where the profiles of $v_{\text{pv}}$, $i_{\text{pv}}$, and $i_g$ are shown. It can be seen that after the MPPT is enabled, the amplitude of $i_g$ gradually increases and settles down after the tracking converges. Also, as the output power increases, the dc value of $v_{\text{pv}}$ gradually declines from OCC voltage to MPP voltage, and the amount of 100 Hz ripple seen in $v_{\text{pv}}$ and $i_{\text{pv}}$ tends to increase. This validates the RGTI operation performing MPPT in grid-tied mode.

After detecting a grid outage, where $f_{\text{grid}} = \text{L}$, the system-level control transitions the RGTI into battery-tied mode and into MPPT submode $R_{B1}$. The control performance in $R_{B1}$ is shown in Fig. 10(b), where the measured profiles of $v_{\text{pv}}$, $i_{\text{pv}}$, and $i_{L1}$ are indicated when MPPT is enabled. The control structure of this mode is indicated in Fig. 7(b), where the MPPT controller continuously varies the PV bus voltage reference from OCC. Correspondingly, $v_{\text{pv}}$ is seen to reduce from OCC voltage and $i_{\text{pv}}$ is seen to increase from zero. These variables eventually reach steady-state values indicating the convergence of MPP tracking.

Fig. 10(c) shows the simulated control performance of the RGTI in battery-tied mode when BEC submode $R_{B2}$ is enabled, where the dynamic responses of $i_B$, $i_{L1}$, and $v_{\text{pv}}$ are shown based

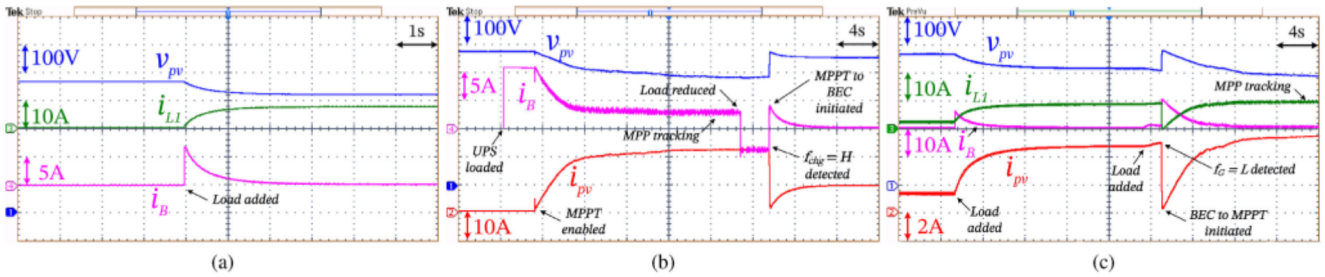


Fig. 11. (a) Experimental battery-current waveforms for a 30% step change in UPS load in BEC submode $R_{B2}$, and submode-transition performance of the RGTI during load transients showing (b) $R_{B1}$ to $R_{B2}$ and (c) $R_{B2}$ to $R_{B1}$ transition.

on the control design carried out in Section VI-C, for a 30% step change in battery load. The two-loop control structure of this mode is indicated in Fig. 7(a). The corresponding experimental waveforms of the battery-current $i_B$ is shown in Fig. 11(a), where a close match in settling times of the two waveforms can be noted. For a step load change, $i_B$ shows a step rise as the battery takes the full load initially. Subsequently, the load disturbance is rejected by the control action and $i_B$ gradually reduces to zero, while the RGTI output inductor current $i_{L1}$ increases proportionally to deliver the required power. Since RGTI functions as a dc–dc converter, $v_{\text{pv}}$ is devoid of 100 Hz ripple unlike the case in grid-tied mode. This validates the capability of RGTI to operate in battery-tied mode with BEC as described in Section VI-A, when solar irradiation is adequate. These results, thus, validate the circuit-level control design of the RGTI in Section VI-C.

In Fig. 11(b), a transition between MPPT and BEC submodes $R_{B1} \rightarrow R_{B2}$ is illustrated. The UPS is loaded at t = 4 s, and as a result, the battery discharges by providing 11 A. The RGTI, which is connected to the battery, is enabled at around t = 8 s. By default, the RGTI enters MPPT mode as explained in Section VIII, and correspondingly $i_B$ magnitude reduces. However, when the load is sufficiently high, the battery continues to discharge even when RGTI performs MPPT, as indicated in Fig. 11(b). At t = 26 s, the UPS load is decreased, and this causes the battery current direction to reverse as the MPP is greater than the UPS load as explained in Section VIII. This condition tends to charge the battery. This is detected by the system-level control, which sets the flag $f_{\text{chg}} = \text{H}$, and the system is subsequently transitioned into BEC mode where the battery current is regulated to zero as seen from the $i_B$ waveform.

In Fig. 11(c), a transition between BEC and MPPT submodes $R_{B2} \rightarrow R_{B1}$ is illustrated. The system is initially operating in BEC mode, as indicated by the nonzero operating values of RGTI output inductor and PV currents $i_{L1}$ and $i_{\text{pv}}$, respectively. At t = 5 s, the UPS load is increased and BEC operation ensures that the battery current is regulated to zero. At t = 24 s, UPS load is further increased and the OPP shifts closer to the MPP of the PV, resulting in a reduction in the power margin below the set threshold. This is detected by the system-level control and the flag $f_G$ is set to low ($f_G = \text{L}$). Correspondingly, the system transitions into the MPPT mode. It can be noticed that the value of $i_{L1}$ when MPP tracking occurs is very close to the value of $i_{L1}$ in BEC mode prior to the mode transition, indicating the close proximity of OPP and MPP, which validates the detection of reduction in PV power margin explained in Section VI-B.

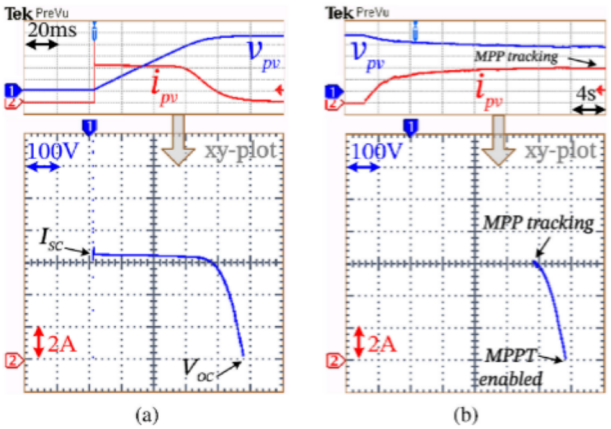


Fig. 12. Experimental $i$–$v$ characteristics of the PV showing (a) during dc bus capacitance charging and (b) during MPPT operation in battery-tied mode.

Fig. 12(a) shows the experimentally measured $i$–$v$ characteristics of the rooftop PV source at a given time of day. Fig. 12(b) shows the corresponding experimental waveform when the RGTI is performing MPPT in battery-tied mode. The characteristics are shown in $xy$-mode, where it can be seen that the PV operating point starts from open-circuit voltage $V_{\text{OC}}$ at OCC, and settles at MPP in steady state, thus validating the MPPT operation.

Fig. 13 shows the transition of RGTI from grid-tied to battery-tied mode $R_G \rightarrow R_{B1}$ under dispersed light conditions, when the grid status flag $f_{\text{grid}}$ turns low ($f_{\text{grid}} = L$) at t = 60 s. The experimentally measured transients in PV voltage $v_{\text{pv}}$, PV current $i_{\text{pv}}$, inductor current $i_{L1}$, and RGTI output node voltage $v_o$ during the mode-transition are shown. The zoomed waveform is also furnished that shows the behavior of the variables during the changeover period. It can be seen that the RGTI performs MPPT in grid-tied mode prior to the changeover. After the mode-transition, as explained in Section VIII, the system by default enters into the MPPT submode $R_{B1}$ of the battery-tied mode. Correspondingly, the variables $v_o$ and $i_{L1}$ change from ac to dc waveforms when the system makes the transition. The MPPT tracking performance can be seen from the profile of the $i_{\text{pv}}$ variable.

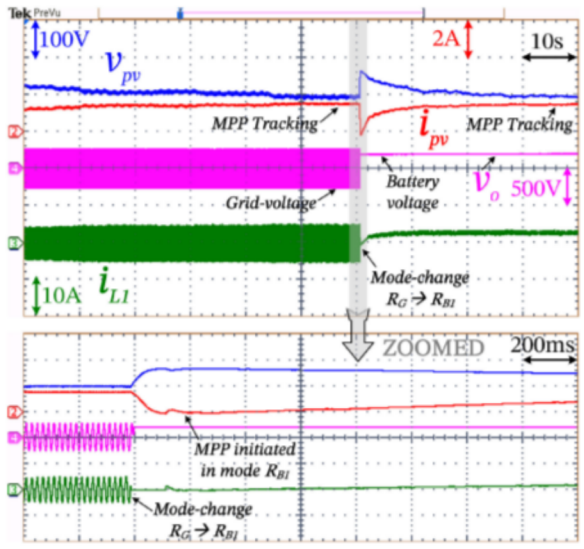


Fig. 13. Experimentally measured profiles of output voltage $v_o$, inductor current $i_{L1}$, and PV voltage and current $v_{\text{pv}}$ and $i_{\text{pv}}$, respectively, during a mode-transition $R_G \rightarrow R_{B1}$.

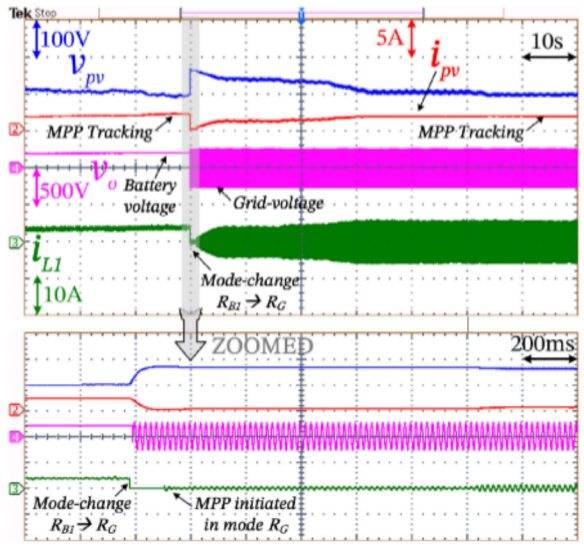


Fig. 14. Experimentally measured profiles of output voltage $v_o$, inductor current $i_{L1}$, and PV voltage and current $v_{\text{pv}}$ and $i_{\text{pv}}$, respectively, during a mode-transition $R_{B1} \rightarrow R_G$.

Fig. 14 shows the reverse transition of RGTI from battery-tied to grid-tied mode $R_{B1} \rightarrow R_G$, when the grid status flag $f_{\text{grid}}$ turns high ($f_{\text{grid}} = H$) at t = 30 s. The corresponding experimentally measured transients in the circuit variables are shown along with the zoomed version during the changeover period. It can be seen that the RGTI functions in the MPPT submode $R_{B1}$ in battery-tied mode prior to the changeover. After the mode-transition, as explained in Section VIII, the system enters into the grid-tied MPPT mode $\mathbf{R_G}$. Correspondingly, the variables $v_o$ and $i_{L1}$ change from dc to ac waveforms, and the MPPT tracking performance is seen from the $i_{\text{pv}}$ profile. These results validate the system-level control and mode-transition table explained in Section VIII.

## X. Conclusion

In this article, an RGTI architecture was proposed, which served as an alternative approach to the hybrid-PV system to access solar energy during a grid outage. The proposed architecture combines the functionalities of the UPS and GTI while keeping the actual systems physically separate and independent in terms of design and control. The operating scheme of such a system was evaluated and it was shown that a dc-coupled configuration of RGTI with an external UPS meets the objectives of independent design and control that does not require high-bandwidth communication links between the UPS and RGTI controllers for operation, unlike an ac-coupled system. The RGTI acts as a regular GTI when the grid is present, but reconfigures as a dc–dc charge-controller during a grid outage and interacts with the battery-bank of an external UPS, thus enabling it to harness solar energy. In order to achieve this objective, circuit-level control using a PV-based battery emulation scheme was proposed. This submode was shown to minimize the discharge burden on the battery during a grid outage whenever solar irradiation was adequate. This submode in conjunction with the conventional MPPT mode was shown to tackle the dynamic variations in UPS load and ambient irradiation conditions, while ensuring that the required energy support was provided from the PV. Discharge of the physical battery was, thus, reduced due to the PV support during an outage, which led to enhanced battery operating life. A system-level supervisory control scheme was proposed that achieved such a functionality by facilitating mode transitions required for overall system operation. Experimental results on a 4 kVA hardware setup in grid-tied and battery-tied modes validated the proposed concept, circuit level, and system-level control designs. Since the design and operation of the RGTI are independent of the external UPS, an existing UPS from any manufacturer can be retrofitted and upgraded with PV capability without interfering with its operation. Such a design approach, thus, leads to enhanced solar energy access during grid outage and increased PV resource utilization similar to a hybrid-PV solution, while also providing features of retrofitting PV and its flexible scaling, to extend the cycle life of the local UPS batteries.

## Acknowledgment

The authors would like to sincerely thank Dr. Anirudh Guha of IIT, Palakkad, and Ms. Roja Peri of IISc, Bangalore, for the technical discussions and valuable inputs.

## References

[1] S. Amamra, K. Meghriche, A. Cherifi, and B. Francois, "Multilevel inverter topology for renewable energy grid integration," *IEEE Trans. Ind. Electron.*, vol. 64, no. 11, pp. 8855–8866, Nov. 2017.

[2] M. Singh, V. Khadkikar, A. Chandra, and R. K. Varma, "Grid interconnection of renewable energy sources at the distribution level with power-quality improvement features," *IEEE Trans. Power Del.*, vol. 26, no. 1, pp. 307–315, Jan. 2011.

[3] H. Jafarian *et al.*, "Design and implementation of distributed control architecture of an ac-stacked PV inverter," in *Proc. IEEE Energy Convers. Congr. Expo.*, Sep. 2015, pp. 1130–1135.

[4] F. Blaabjerg, R. Teodorescu, M. Liserre, and A. V. Timbus, "Overview of control and grid synchronization for distributed power generation systems," *IEEE Trans. Ind. Electron.*, vol. 53, no. 5, pp. 1398–1409, Oct. 2006.
[5] B. Karanayil, V. G. Agelidis, and J. Pou, "Performance evaluation of three-phase grid-connected photovoltaic inverters using electrolytic or polypropylene film capacitors," *IEEE Trans. Sustain. Energy*, vol. 5, no. 4, pp. 1297–1306, Oct. 2014.
[6] E. Koutroulis and F. Blaabjerg, "Design optimization of transformerless grid-connected PV inverters including reliability," *IEEE Trans. Power Electron.*, vol. 28, no. 1, pp. 325–335, Jan. 2013.
[7] R. Teodorescu, M. Liserre, P. Rodriguez, and F. Blaabjerg, *Grid Converters for Photovoltaic and Wind Power Systems*, vol. 29. Hoboken, NJ, USA: Wiley, 2011.
[8] P. Du, Z. Ye, E. E. Aponte, J. K. Nelson, and L. Fan, "Positive-feedback-based active anti-islanding schemes for inverter-based distributed generators: Basic principle, design guideline and performance analysis," *IEEE Trans. Power Electron.*, vol. 25, no. 12, pp. 2941–2948, Dec. 2010.
[9] *IEEE Standard for Interconnecting Distributed Resources With Electric Power Systems*, IEEE Standard 1547-2018, May 2018.
[10] J. Park, J. Kwon, E. Kim, and B. Kwon, "High-performance transformerless online UPS," *IEEE Trans. Ind. Electron.*, vol. 55, no. 8, pp. 2943–2953, Aug. 2008.
[11] S. S. H. Bukhari, T. A. Lipo, and B. Kwon, "An online UPS system that eliminates the inrush current phenomenon while feeding multiple load transformers," *IEEE Trans. Ind. Appl.*, vol. 53, no. 2, pp. 1149–1156, Mar. 2017.
[12] L. Arnedo, S. Dwari, V. Blasko, and A. Kroeber, "Hybrid solar inverter based on a standard power electronic cell for microgrids applications," in *Proc. IEEE Energy Convers. Congr. Expo.*, 2011, pp. 961–967.
[13] L. Arnedo, S. Dwari, V. Blasko, and S. Park, "80 kW hybrid solar inverter for standalone and grid connected applications," in *Proc. IEEE Appl. Power Electron. Conf. Expo.*, Feb. 2012, pp. 270–276.
[14] S. Dwari, L. Arnedo, and V. Blasko, "Advanced techniques for integration of energy storage and photovoltaic generator in renewable energy systems," in *Proc. IEEE Energy Convers. Congr. Expo.*, Sep. 2014, pp. 395–401.
[15] C. Cavallaro, S. Musumeci, C. Santonocito, and M. Pappalardo, "Load priority control strategy for SPV-UPS system," in *Proc. IEEE, Power Electron. Electr. Drives Autom. Motion*, 2010, pp. 1207–1212.
[16] C. Wen and J. Jia, "Research and analysis of the improved inverse-droop control strategy for dual mode inverters in micro grid," in *Proc. IET Electr. Eng. Academic Forum, Tsinghua University*, May 2016, pp. 1–6.
[17] Shatakshi, B. Singh, and S. Mishra, "Dual mode operational control of single stage PV-battery based microgrid," in *Proc. IEEMA Engineer Infinite Conf.*, Mar. 2018, pp. 1–5.
[18] T. Hirose and H. Matsuo, "Standalone hybrid wind-solar power generation system applying dump power control without dump load," *IEEE Trans. Ind. Electron.*, vol. 59, no. 2, pp. 988–997, Feb. 2012.
[19] M. Rezkallah, A. Hamadi, A. Chandra, and B. Singh, "Design and implementation of active power control with improved P&O method for wind-pv-battery-based standalone generation system," *IEEE Trans. Ind. Electron.*, vol. 65, no. 7, pp. 5590–5600, Jul. 2018.
[20] I. Sulaeman, V. Vega-Garita, G. R. C. Mouli, N. Narayan, L. Ramirez-Elizondo, and P. Bauer, "Comparison of PV-battery architectures for residential applications," in *Proc. IEEE Int. Energy Conf.*, Apr. 2016, pp. 1–7.
[21] J. Sridhar, G. R. C. Mouli, P. Bauer, and E. Raaijen, "Analysis of load shedding strategies for battery management in PV-based rural off-grids," in *Proc. IEEE Eindhoven PowerTech*, Jun. 2015, pp. 1–6.
[22] H.-S. Ban, J.-M. Lee, H.-S. Mok, and G.-H. Choe, "Load sharing improvement in parallel-operated lead acid batteries," in *Proc. IEEE Int. Symp. Ind. Electron.*, Jun. 2001, vol. 2, pp. 1026–1031.
[23] S. Karve, "Three of a kind UPS topologies, IEC standard," *IEE Rev.*, vol. 46, no. 2, pp. 27–31, Mar. 2000.
[24] B. Yang, W. Li, Y. Gu, W. Cui, and X. He, "Improved transformerless inverter with common-mode leakage current elimination for a photovoltaic grid-connected power system," *IEEE Trans. Power Electron.*, vol. 27, no. 2, pp. 752–762, Feb. 2012.
[25] F. El Aamri, H. Maker, D. Sera, S. V. Spataru, J. M. Guerrero, and A. Mouhsen, "A direct maximum power point tracking method for single-phase grid-connected PV inverters," *IEEE Trans. Power Electron.*, vol. 33, no. 10, pp. 8961–8971, Oct. 2018.
[26] R. W. Erickson and D. Maksimovic, *Fundamentals of Power Electronics*. New York, NY, USA: Springer, 2007.
[27] D. N. Zmood and D. G. Holmes, "Stationary frame current regulation of pwm inverters with zero steady state error," in *Proc. IEEE Power Electron. Spec. Conf.*, Jul. 1999, vol. 2, pp. 1185–1190.
[28] F. de Bosio, M. Pastorelli, L. A. D. S. Ribeiro, M. S. Lima, F. Freijedo, and J. M. Guerrero, "Current control loop design and analysis based on resonant regulators for microgrid applications," in *Proc. IEEE Ind. Electron. Soc. Conf.*, Nov. 2015, pp. 005322–005327.
[29] A. F. Hoke, M. Shirazi, S. Chakraborty, E. Muljadi, and D. Maksimovic, "Rapid active power control of photovoltaic systems for grid frequency support," *IEEE J. Emerg. Sel. Topics Power Electron.*, vol. 5, no. 3, pp. 1154–1163, Sep. 2017.
[30] T. Esram and P. L. Chapman, "Comparison of photovoltaic array maximum power point tracking techniques," *IEEE Trans. Energy Convers.*, vol. 22, no. 2, pp. 439–449, Jun. 2007.
[31] D. Venkatramanan and V. John, "Dynamic modeling and analysis of buck converter based solar PV charge controller for improved MPPT performance," *IEEE Trans. Ind. Appl.*, vol. 55, no. 6, pp. 6234–6246, Nov. 2019.
[32] N. Femia, G. Petrone, G. Spagnuolo, and M. Vitelli, *Power Electronics and Control Techniques for Maximum Energy Harvesting in Photovoltaic Systems*. Boca Raton, FL, USA: CRC Press, 2017.

**D. Venkatramanan** (S'18) received the B.Tech. degree in electrical and electronics engineering from the National Institute of Technology, Trichy, India, in 2008, and the M.E. degree in electrical engineering in 2010 from the Indian Institute of Science, Bangalore, India, where he is currently working toward the Ph.D. degree in electrical engineering.

He was a Design Engineer with Schneider Electric India Pvt. Ltd, in the uninterruptible power supply division from 2010 to 2013, and an Electrical Engineer with General Electric Healthcare, Bangalore, from 2013 to 2014. His current research interests include design and control of solar photovoltaic systems, energy storage systems, pulsewidth modulation filters, and grid-integration of renewables.

**Vinod John** (SM'07) received the B.Tech. degree in electrical engineering from the Indian Institute of Technology Madras, Chennai, India, in 1992, the M.S.E.E. degree from the University of Minnesota, Minneapolis, MN, USA, in 1994, and the Ph.D. degree from the University of Wisconsin-Madison, Madison, WI, USA, in 1999, both in electrical engineering.

He has worked in research and development positions with the GE Global Research, Niskayuna, NY, USA, and Northern Power, Barre, VT, USA. He is currently an Associate Professor with the Department of Electrical Engineering, Indian Institute of Science, Bengaluru, India. His research interests include power electronics and distributed generation, power quality, high-power converters, and motor drives.